Wall-Sticking Drone for Non-Destructive Inspection of Oblique Planes

Menglong Zhou, Zhi An, and Nak Young Chong*
School of Information Science
Japan Advanced Institute of Science and Technology
Nomi, Ishikawa 923-1292, Japan
{s2020410, an-zhi, nakyoung}@jaist.ac.jp

***Abstract*—This paper discusses the preliminary design and analysis of a light-duty unmanned aerial vehicle (UAV) for remote inspection operations. Due to limitations in payload capacity and energy supply, small drones are often employed in distant visual inspection tasks. We propose a novel UAV landing gear system for non-destructive testing operations on carbon steel spherical storage tanks. The landing gear system employs a servo motor as the power source. It utilizes a combination of slider crank and gear mechanisms for controlling the orientation of the magnetic grippers, enabling adhesion in conjunction with UAV flight. Additionally, the system incorporates a cost-effective and lightweight switchable magnetic adhesion method based on neodymium magnets and silicon steel sheets to reduce weight, which can provide 37.72N per unit. The system's total weight is approximately 1.6kg, with a payload capacity of 400g. The proposed prototype design has sufficient payload capacity to carry standard non-destructive testing probes, such as ultrasonic and electromagnetic, supported by empirical evidence obtained through our in-house experiments.**

***Index Terms*—UAV, wall-sticking drone, non-destructive testing, magnetic gripper, landing gear system**

I. Introduction

Spherical tanks are primarily used in industries to store gases and liquefied gases. The execution of regular safety and quality testing procedures is paramount for ensuring safe production. Similar to tasks such as bridge inspection and ship inspection, using robotic platforms instead of manual labor for pressure vessel inspection has consistently been a crucial undertaking because the robotic platforms approach can save costs and time and keep operators from potential hazards. Among existing robotic platforms, drones offer the unique ability to inspect container surfaces from a distance and perform localized, close-up inspection operations. This paper proposed a new drone system for spherical tank inspection.

In recent years, legal restrictions on UAVs have become increasingly stringent in various countries, and practitioners may face increased learning costs. Lighter and smaller UAVs are more portable and subject to looser regulations (some countries require different levels of pilot licenses to operate drones based on their size and carrying weight). Thus, the F450 drone, with a maximum carrying weight of $2kg$, is chosen as the research platform for this paper. Taking spherical carbon steel pressure vessels as an example, the challenges of this task primarily stem from the following aspects:

- From the perspective of inspected objects, the landing gear mechanism needs to orient the magnetic gripper to any angle between 0 and 180 degrees while being as lightweight as possible to adhere to any point on the spherical pressure vessel.
- From the perspective of structure design, the F450 has a small payload capacity, requiring a simple and lightweight structure. Firstly, from the UAV's top-down view, the spacing between propellers is only 68.7mm. Therefore, the mechanism design should not be too close to the propellers to avoid potential hazards. Additionally, servos positioned closer to the UAV's center of mass result in minimal impact on the UAV's flight attitude due to mechanical deformation under flight conditions. However, from a side view, it can be observed that to safely maneuver the magnetic gripper mechanism around the propellers, the maximum distance from the propellers is longer than the distance of a 90-degree position.
- From the perspective of the power module, the power module of the F450 UAV is also limited. Attachment methods such as electromagnets or vacuum magnetic grippers, which require a long-term power supply, are unsuitable when using systems for non-destructive testing operations.

Therefore, this paper proposes a wall-sticking drone for non-destructive inspection, using servos as power sources, with a crank-slider mechanism and gear mechanism serving as the angle control module. Additionally, we introduce a simple and cost-effective permanent magnet adhesion structure as the magnetic gripper module to reduce the impact of the UAV's weight on the system. Our design, including the F450 and flight controller battery components, only has a total weight of 1.6kg. The drone we designed is divided into four parts, as shown in Fig. 1. It's important to note that the sensors include not only those commonly used for non-destructive testing, such as ultrasonic probes or electromagnetic probes, but can also accommodate devices like RGB-D cameras to enhance the UAV's operational accuracy. We aim to design a drone that can stick to any selected point inside or outside the spherical tank as required, as shown in Fig. 2. The landing gear system only needs to account for changes in the pitch angle, denoted by β, when the UAV is in flight mode.

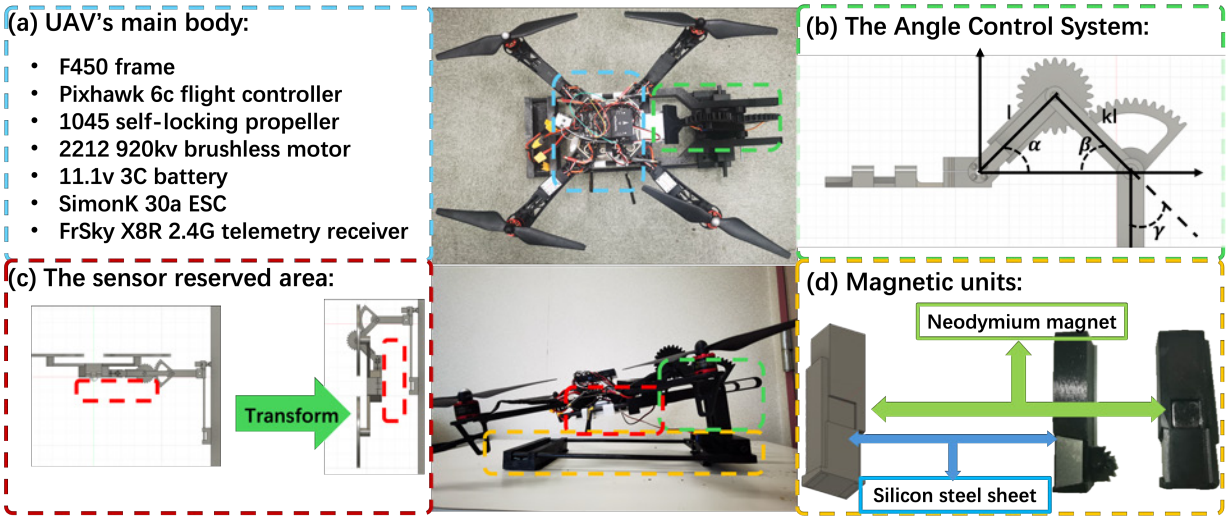

Fig. 1. Four components of our proposed UAV: (a) the main body of the UAV, (b) the angle control system, (c) the reserved area for sensors, and (d) the magnetic unit.

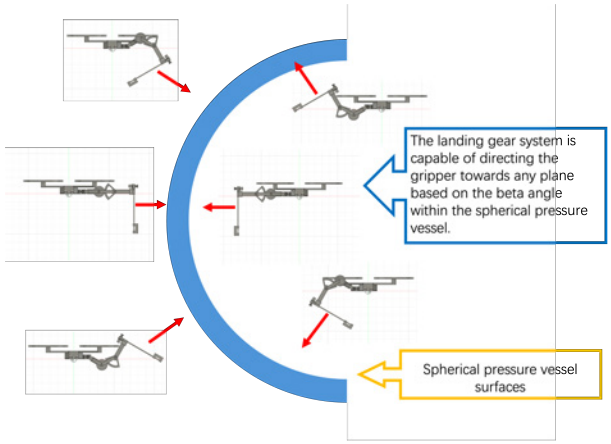

Fig. 2. This figure illustrates a hemisphere, representing the surface of a hemispherical pressure vessel.

The spherical pressure vessel is constructed from multiple metal plates welded together [1], [2]. During inspection tasks, sensors operate along the weld seams [3]. Thus, in this task, the primary variations of the proposed landing gear system occur in the beta angle. Concurrently, the drone's flight orientation can be adjusted to change the alpha angle. Changes in the gamma angle are not considered. This system positions the designated sensors directly underneath the drone. This area remains parallel to the spherical tank's surface during the adhesion, ensuring the drone maintains a consistent distance from the wall at the final position. In other words, the sensors consistently preserve a specific gap from the wall, regardless of the angle of adhesion.

II. RELATED WORK

Non-destructive testing operations are necessary to prevent major accidents in structures such as bridges [4], [5], pressure vessels [6], [7], and ships [8], [9]. Typically, these inspections require personnel to erect scaffolding or use aerial work platforms in hazardous environments. Therefore, UAVs have been widely applied in the inspection as platforms capable of navigating terrain obstacles.

In [10], a scheme for visual detection is proposed, with [11] building upon it. By utilizing an octo-rotor UAV, vertical forces can be applied to different inclines by controlling the UAV's flight attitude. Such tasks require the UAV to hover in the air. In [12], a platform for a hexa-rotor UAV is devised, featuring a hybrid rolling-aerial platform design. This platform can land and move along pipes during inspection without wasting energy on the propellers. Similarly, [13] proposes a landing gear mechanism for quad-rotor UAVs to facilitate their docking on surfaces. In [14], electromagnets and a set of suspension devices are used to provide a stable platform during the detection process, ensuring the sensor is not affected by external disturbances to the drone.

However, regardless of the inspection task, the target surface often includes both vertical and horizontal elements. Providing a surface parallel to this plane is necessary during operations. In this aspect, the final posture of most climbing robots has an advantage. According to adhesion principles, climbing mechanisms can be classified into magnetic adhesion, negative pressure adhesion, and magnetic gripper adhesion, among others [15]. Due to having four rotors as power sources, UAVs are often designed as negative-pressure suction robots [16]. Among them, permanent magnetic adhesion robots are particularly popular. Magnetic tread climbing robots [17]–[20] and wheeled climbing robots [21], [22] can bear high load capacities and also possess functions such as climbing slopes and overcoming obstacles.

This study integrates magnetic adhesion into the landing gear system, rotating the system to a uniform state after adhesion. With the UAV as a reference, the inspected surface

is uniformly arranged into a plane in the same direction, simplifying issues such as designing mechanical arms.

III. STRUCTURE DESIGN FOR ROBOTIC LANDING GEAR

The robot's landing gear system consists of three components: the angle control system, the magnetic adhesion system, and the sensor reserved area. Through angle control, the orientation of the mechanical legs can be adjusted from 0 to 180 degrees. Utilizing the magnetic adhesion system, the UAV can adhere to surfaces at any angle within a spherical tank. After the UAV lands, the angle control system will return to its initial 0-degree state. Even if the power is disconnected, the magnetic adhesion system can still maintain the adhesion state until the task is completed. We also reserve an area for users to accommodate a variety of sensors according to their tasks.

A. The Angle Control System

This part includes a crank-slider mechanism and a gear mechanism used to position the magnetic gripper in the desired direction, as shown in Fig. 2. To facilitate a more intuitive analysis, we constructed a 3D model as depicted in Fig. 1(b). A complex plane and Cartesian coordinates are introduced to define the coordinate system, with the origin set at the center of the servo motor. One side of the crank-slider mechanism is defined as l, and the other is as kl. The angular displacement of the servo motor, denoted by α, is used to derive other angular relationships through the following formulas. In this task, α reaches its maximum positive and negative values when the end of the mechanical leg needs to orient towards positive and negative 90 degrees, respectively, as shown in Eq. 1-3.

$$\frac{\sin\alpha}{l} = \frac{\sin\beta}{kl} \tag{1}$$

$$\beta = \arcsin\left(k\sin\alpha\right) \tag{2}$$

$$\gamma = 90^\circ - \beta \tag{3}$$

During the design process, the maximum distance required by the mechanism was known. Therefore, to facilitate the design, we simplified Eq. 1-3 into a function of α and k, as shown in Eq. 4. This approach allows us to focus solely on the servo's turning angle (α) and the ratio of lengths between joints (k). It is also noted that the smaller the α, the lower the system's resolution. In this paper, to balance the resolution while reducing weight, we ultimately selected a design with k equal to 1 and α set to 90 degrees.

$$f\left(\alpha, k\right) = \frac{\alpha + \arcsin\left(k\sin\alpha\right)}{90^\circ - \arcsin\left(k\sin\alpha\right)} \tag{4}$$

B. The Magnetic Adhesion System

This part consists of three components: the magnetic unit, the switching mechanism, and the end friction mechanism:

The magnetic unit comprises neodymium magnets and silicon steel sheets. Neodymium magnets, with $10mm$ edge lengths, serve as the magnetic source. The poles of the magnets are directed towards the adhesion surface through silicon steel sheets measuring $25mm$ in length, $10mm$ in width, and $2.5mm$ in thickness. Due to the excellent magnetic permeability of the silicon steel sheets, a magnetic circuit is formed upon contact with the adhesion surface, thereby adhering the mechanism to the surface. Two magnetic units are employed in the magnetic gripper system, as illustrated in Fig. 1(d).

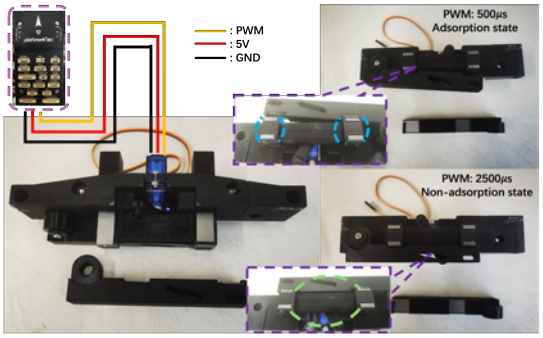

Fig. 3. The structure of the magnetic gripper.

The switch mechanism employs another two sets of silicon steel plates in contact with two magnetic units. Their north and south poles are interconnected, resulting in a significant reduction in adhesive force to the iron plate. This paper constructs the switch mechanism and proposes a small servo motor as the power source. The silicon steel plates employ silicon steel plates measuring $57mm$ in length, $13mm$ in width, and $2.5mm$ in thickness, controlled by a lever to engage or disengage the adhesion as shown in Fig. 3.

The working principle of the magnetic gripper operating through a servo motor switch. It alters the servo's angle to establish or interrupt the externally applied magnetic flux path provided by the mechanism. In the adsorption state, the magnet forms a magnetic circuit through the silicon steel sheet and the iron plate (highlighted in blue), resulting in a strong suction force. In the non-absorption state, the two sets of magnetic units are interconnected by an additional external silicon steel sheet (highlighted in green), forming a magnetic circuit that significantly reduces the suction force.

The end friction mechanism comprises two sets of magnet arrays separated by anti-skid rubber. This mechanism remains in an adhesive state, providing the required force at different angles, and adheres to the surface being attracted as an auxiliary magnetic mechanism.

C. The Sensor Reserved Area

This part is located directly beneath the UAV and can accommodate various sensors according to specific requirements.

Simultaneously, an RGB-D visual module can be installed in this part area, serving as an image transmission module during normal UAV flight. Upon nearing the adhesion surface, utilizing the depth camera for precise angle calculations can significantly improve adhesion success rates.

IV. EXPERIMENTS

In the experiments, we will discuss two tasks: the adhesion task and the structural analysis task.

In the adhesion task, we qualitatively analyze the suction force of the magnetic unit. In the experiment, a robotic arm vertically attaches the magnetic mechanism to an iron plate. Using the robotic arm's built-in force sensor makes the sensor value negative when the arm compresses the mechanism. The arm is slowly raised until the tested mechanism detaches from the iron plate. The maximum sensor value indicates the maximum suction force the magnetic mechanism provides, as shown in Fig. 4.

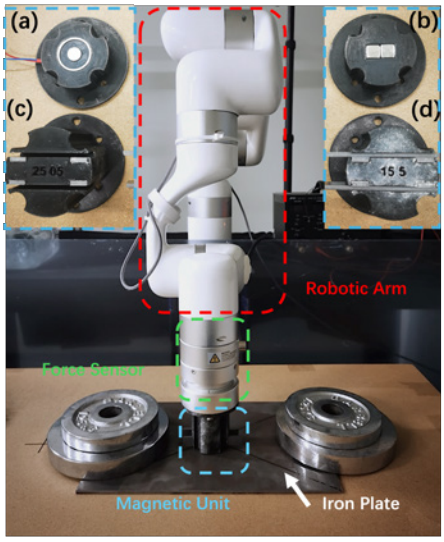

Fig. 4. The robotic arm device used for the experiment performs reciprocating tests on the suction gripping mechanism to determine the maximum suction force.

The experimental apparatus utilized in our study is shown in Fig. 4. The red highlighted indicates the robotic arm employed. The green highlight indicates the built-in force sensors within the robotic arm. The magnetic units under test are accentuated in blue. We prepared four types of magnetic units for testing: our proposed magnetic unit in both the adhesion state (c) and non-adhesion state (d), an electromagnet (a), and a magnetic unit composed of two neodymium magnets (a). It is important to note that the neodymium magnet unit was fabricated by gluing two magnets together in the same polarity orientation within a mold. When this assembly directly adheres to an iron plate, it can achieve the maximum magnetic force offered by a unit composed of two neodymium magnets.

In order to ensure data reliability, each device underwent 500 consecutive experiments. The top three maximum values were averaged to represent a single data point. The average and standard deviation, denoted by σ, were then calculated. As shown in Fig 5, the highlighted segments denote critical phases of the experiment: the first inflection point (yellow) signifies the moment when the magnetic unit descends sufficiently close to the iron plate, causing the plate to deform and adhere to the unit. The second inflection point (green) is artificially established, indicating the juncture where the robotic arm presses the mechanism against the iron plate with a predefined force of -30N. The third inflection point (blue) represents the maximum force in the adhesion state of the magnet, which is the experimental data of interest measured in newtons (N).

After conducting the experiment, we found that each magnetic unit we designed can provide a force of $37.72N$ (σ: 2.24) in the adsorption state. Additionally, the unit retains a residual force of $1.21N$ (σ: 0.74) upon disconnection. Additionally, it is observed that two neodymium magnets weighing only $24g$ can provide a force of 62.64N (σ: 2.54), which is comparable to the 63.46N (σ: 5.28) force provided by a $5V$ electromagnet weighing $47g$, yet with more excellent stability.

In the structural analysis task, we first depict the force analysis diagram of the magnetic gripper in the deformation tasks. As shown in Fig. 7, when the magnetic gripper is magnetically attached to a surface, the influence of torque can be disregarded here (assuming that a significant torque is generated, the UAV may detach).

$$F1' = F1 + F3 \tag{5}$$

$$F2' = F2 + F4 \tag{6}$$

In Eq. 5, $F1'$ represents the attractive force provided by the mechanism, while in Eq. 6, $F2'$ represents the frictional force required during the adsorption by the mechanism. The system transitions to an inspection state once the drone has landed (taking 90 degrees as an example). At this juncture, the capabilities of the magnetic gripper are maximized to ensure that the system adheres to the iron plate and can withstand the pressure necessary for the use of the carried sensors during detection. In order to address the complexity, it is acknowledged that the predominant source of magnetic force is attributed to $F1$, as shown by the top magnetic unit in Fig. 7. This force is significantly large, ensuring that the mechanism neither slides nor falls off the wall. Consequently, the problem can be simplified to the following formula.

$$G \cdot L1 \cdot \sin\alpha = F1 \cdot L2 \tag{7}$$

$$L1 = \frac{L3}{\sin\beta} \tag{8}$$

$$G \cdot L3 \cdot \frac{\sin\alpha}{\sin\beta} = F1 \cdot L2 \tag{9}$$

When the angle between the direction of gravity and $L1$ is represented by α, Eq. 5 can be obtained. As depicted in the figure, in this scenario, α equals β. After determining the

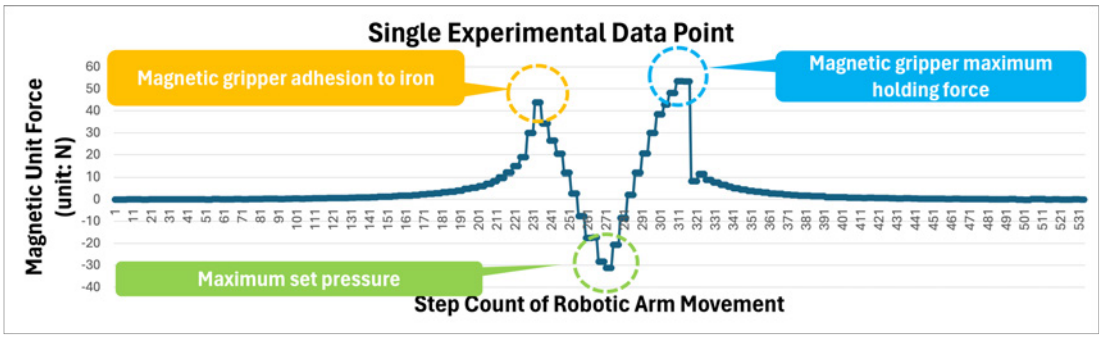

Fig. 5. A detailed view of a single data point from the testing of a magnetic unit.

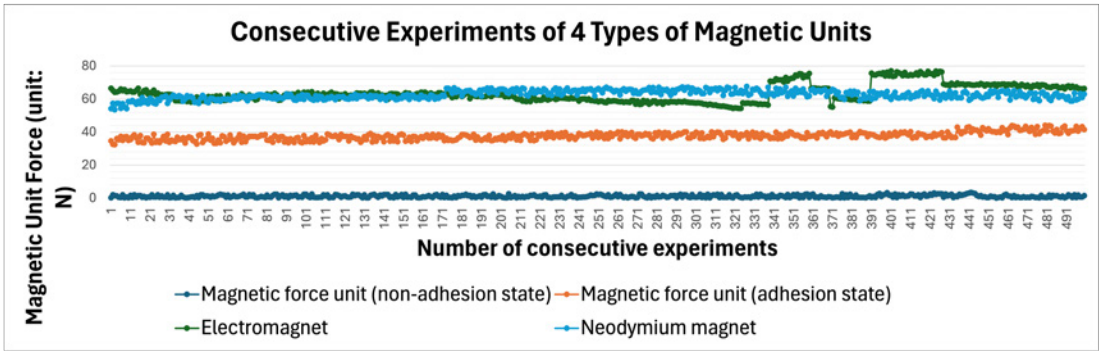

Fig. 6. The performance of four different magnetic units across a series of consecutive experiments. Notably, the magnetic force units exhibit differing behaviors in adhesion and non-adhesion states, suggesting variations in magnetic efficiency under these conditions.

dimensions of the magnetic gripper mechanism, Eq. 7 holds under any circumstances where all parameters are positive values. Since $F1$ is directly proportional to $L3$, reducing $L3$ can decrease the force at the suction point during operation, making it more suitable for UAV work. Therefore, in the design, we employed a slider-crank mechanism and used a gear mechanism to restrict its working range between positive and negative 45 degrees, preventing the mechanism from locking up. Compared to the structure directly using a servo motor and magnetic gripper mechanism with a single rigid leg, our structure's distance in the adhesion state is only $141.4mm$.

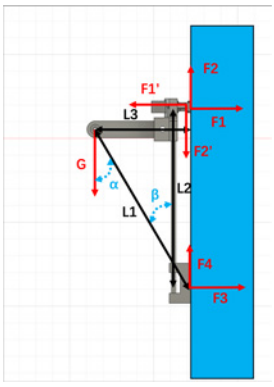

Fig. 7. Force analysis of a magnetic gripper mechanism in an adhesion state within a 3D modeling environment.

Finally, to simulate the surfaces of the pressure vessel at different angles, we utilize a robotic arm equipped with an iron plate, as illustrated in Fig. 8. The structure of the pressure vessel allows us to determine the exact latitudes and longitudes for inspection, along with the necessary pitch angle. After adjusting its landing gear system to achieve the required angle, the UAV slowly contours to approach the iron plate. Once it reaches the designated position, the gripper switch is engaged to activate the adsorption state. Subsequently, the UAV's power is deactivated, and the system is switched to inspection mode. Following the inspection, the landing gear system reverts to flight mode, realigning the UAV horizontally. Power is restored, and as the propellers generate sufficient lift, the gripper's adsorption state disengages.

V. CONCLUSIONS AND FUTURE WORK

This study introduced a novel UAV landing gear system designed specifically for non-destructive testing operations on carbon steel spherical storage tanks. Powered by a servo motor, the landing gear system employs a combination of slider crank and gear mechanisms to control the orientation of magnetic grippers, facilitating adhesion during UAV flight. With a total weight of approximately $1.6kg$ and a payload capacity of $400g$, the system can effectively accommodate standard non-destructive testing probes such as ultrasonic and electromagnetic, thus offering a viable solution for industrial inspection tasks.

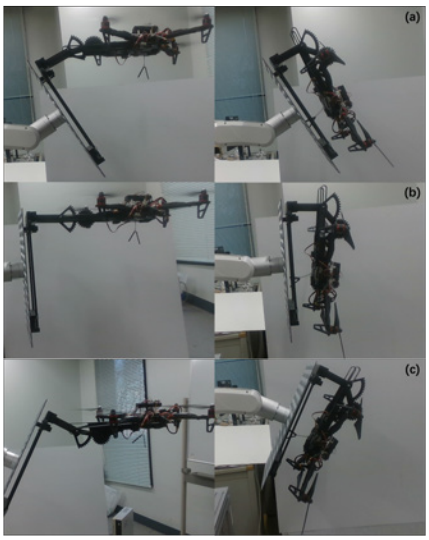

Fig. 8. This figure illustrates the proposed adsorption posture (on the left side) and non-destructive inspection working posture (on the right side) at various angles. We simplified the wall of the spherical pressure vessel and the horizontal angle (β), both internal and external, into three scenarios: (a) less than 90 degrees; (b) 90 degrees; (c) more than 90 degrees.

Although this study provides a novel solution for non-destructive inspection tasks, there are several avenues for future research that could build upon our findings. Firstly, in the design of climbing robot machines, using permanent magnets as an adhesion method has always been a hot topic of discussion. For example, techniques such as using the Halbach arrays to increase magnetic force or using aluminum-nickel-cobalt alloys to produce electric permanent magnet units have been explored. We have proposed a cost-effective and lightweight approach to the on-off control of magnetic force using permanent magnets. However, in this experiment, we still used magnetic units without switch functionality to provide higher adhesion capability, requiring larger forces for the mechanism to detach from the adhesion surface. If a switch similar to the Halbach array could be incorporated into the production process, it would provide more reliable adhesion capability.

Finally, UAVs can exert forces at different angles while moving. The mechanism can be simplified if it doesn't rely on a servomotor but rather on the UAV's motion control to activate and deactivate the adhesion method. Such a mechanism could be used on lighter UAVs as an adhesion method device for wall-parking tasks.

ACKNOWLEDGMENT

This work was supported by the Asian Office of Aerospace Research and Development under Grant/Cooperative Agreement Award No. FA2386-22-1-4042.

REFERENCES

[1] Z. Yang, D. Zhang, L. Guo, B. Yang, and G. Wang, "Seismic performance analysis of the large spherical tank," in *Pressure Vessels and Piping Conference*, vol. 46001. American Society of Mechanical Engineers, 2014, p. V003T03A047.

[2] F. Ji, X. Wang, G. Deng, J. Feng, and H. Liang, "Effect of the shapes of diversion umbrellas on temperature field in a large spherical tank during heat treatment processes," in *Pressure Vessels and Piping Conference*, vol. 56956. American Society of Mechanical Engineers, 2015, p. V002T02A022.

[3] L. Lan, W. Zhang, P. Liu, and L. Si, "Weld recognition of pressure vessel based on texture feature," in *2021 6th International Conference on Intelligent Computing and Signal Processing (ICSP)*. IEEE, 2021, pp. 1331–1335.

[4] M. Aliyari, E. L. Droguett, and Y. Z. Ayele, "Uav-based bridge inspection via transfer learning," *Sustainability*, vol. 13, no. 20, p. 11359, 2021.

[5] Z. Ameli, Y. Aremanda, W. A. Friess, and E. N. Landis, "Impact of uav hardware options on bridge inspection mission capabilities," *Drones*, vol. 6, no. 3, p. 64, 2022.

[6] C. J. O. Salaan, Y. Okada, S. Mizutani, T. Ishii, K. Koura, K. Ohno, and S. Tadokoro, "Close visual bridge inspection using a uav with a passive rotating spherical shell," *Journal of Field Robotics*, vol. 35, no. 6, pp. 850–867, 2018.

[7] R. V. Espinoza, A. S. de Oliveira, L. V. R. de Arruda, and F. N. Junior, "Navigation's stabilization system of a magnetic adherence-based climbing robot," *Journal of Intelligent & Robotic Systems*, vol. 78, pp. 65–81, 2015.

[8] M. Ahmed, M. Eich, and F. Bernhard, "Design and control of mira: A lightweight climbing robot for ship inspection," *International Letters of Chemistry, Physics and Astronomy*, vol. 55, pp. 128–135, 2015.

[9] M. Eich, F. Bonnin-Pascual, E. Garcia-Fidalgo, A. Ortiz, G. Bruzzone, Y. Koveos, and F. Kirchner, "A robot application for marine vessel inspection," *Journal of Field Robotics*, vol. 31, no. 2, pp. 319–341, 2014.

[10] N. Metni and T. Hamel, "A uav for bridge inspection: Visual servoing control law with orientation limits," *Automation in construction*, vol. 17, no. 1, pp. 3–10, 2007.

[11] T. Ikeda, S. Yasui, M. Fujihara, K. Ohara, S. Ashizawa, A. Ichikawa, A. Okino, T. Oomichi, and T. Fukuda, "Wall contact by octo-rotor uav with one dof manipulator for bridge inspection," in *2017 IEEE/RSJ International Conference on Intelligent Robots and Systems (IROS)*. IEEE, 2017, pp. 5122–5127.

[12] A. Suarez, A. Caballero, A. Garofano, P. J. Sanchez-Cuevas, G. Heredia, and A. Ollero, "Aerial manipulator with rolling base for inspection of pipe arrays," *IEEE Access*, vol. 8, pp. 162 516–162 532, 2020.

[13] T. Huang, A. Elibol, and N. Y. Chong, "Enabling landings on irregular surfaces for unmanned aerial vehicles via a novel robotic landing gear," *Intelligent Service Robotics*, vol. 15, no. 2, pp. 231–243, 2022.

[14] R. A. Mattar and R. Kalai, "Development of a wall-sticking drone for non-destructive ultrasonic and corrosion testing," *Drones*, vol. 2, no. 1, p. 8, 2018.

[15] Y. Fang, S. Wang, Q. Bi, D. Cui, and C. Yan, "Design and technical development of wall-climbing robots: A review," *Journal of Bionic Engineering*, vol. 19, no. 4, pp. 877–901, 2022.

[16] S. Mahmood, S. Bakhy, and M. Tawfik, "Propeller-type wall-climbing robots: A review," in *IOP Conference Series: Materials Science and Engineering*, vol. 1094, no. 1. IOP Publishing, 2021, p. 012106.

[17] J. Hu, X. Han, Y. Tao, and S. Feng, "A magnetic crawler wall-climbing robot with capacity of high payload on the convex surface," *Robotics and Autonomous Systems*, vol. 148, p. 103907, 2022.

[18] C. Yan, Z. Sun, W. Zhang, and Q. Chen, "Design of novel multidirectional magnetized permanent magnetic adsorption device for wall-climbing robots," *International Journal of Precision Engineering and Manufacturing*, vol. 17, pp. 871–878, 2016.

[19] F. Gao, J. Fan, L. Zhang, J. Jiang, and S. He, "Magnetic crawler climbing detection robot basing on metal magnetic memory testing technology," *Robotics and Autonomous Systems*, vol. 125, p. 103439, 2020.

[20] Z. Zhao, Y. Tao, J. Wang, and J. Hu, "The multi-objective optimization design for the magnetic adsorption unit of wall-climbing robot," *Journal of Mechanical Science and Technology*, vol. 36, no. 1, pp. 305–316, 2022.

[21] S. Jiao, X. Zhang, X. Zhang, J. Jia, and M. Zhang, "Magnetic circuit analysis of halbach array and improvement of permanent magnetic adsorption device for wall-climbing robot," *Symmetry*, vol. 14, no. 2, p. 429, 2022.

[22] W. Song, Z. Wang, T. Wang, D. Ji, and S. Zhu, "A path tracking method of a wall-climbing robot towards autonomous inspection of steel box girder," *Machines*, vol. 10, no. 4, p. 256, 2022.